JOURNAL OF MATERIALS SCIENCE **39** (2004) 1523– 1526

A study on the corrosion behavior of nanostructured electrodeposited cobalt

A. ALEDRESSE
School of Engineering, Laurentian University, Sudbury, Ontario, Canada

A. ALFANTAZI*
Dept. of Metals and Materials Engineering, University of British Columbia, Vancouver, BC, Canada
E-mail: alfantaz@interchange.ubc.ca

Chromium coatings are used to impart corrosion resistance to components in many industrial applications. Typically these coatings are produced from hexavalent chromium plating baths [1]. However, hexavalent chromium has been shown to increase the risk of cancer to the lung and nose in personnel working in plating shops [2]. In addition to the health risks associated with chromium plating, there are several technical drawbacks to this technology including the relatively low plating efficiency [3]. Also, high rates of hydrogen generation occur and precautions must be taken to prevent hydrogen embrittlement of susceptible substrate materials. The development of alternative technology to chromium plating involves a number of technical challenges. Most research efforts over the past few years have been concentrated on the production of nanocrystalline materials. Recent efforts on property characterization of these materials have revealed that they have unique properties as a result of microstructural differences compared with their conventional coarse grained or amorphous counterparts. On account of a good corrosion resistance, electro-plating with nanocrystalline cobalt is of considerable practical interest and expected to provide the best alternative to chromium [3]. The overall objective of the current research is to evaluate the corrosion behavior of electrodeposited nanostructured Co and Co-P alloy in alkaline media using potentiodynamic polarization.

In the current study, three different working electrodes were used. The first was industrially produced polycrystalline cobalt which was provided by Falconbridge Ltd. with purity of 99.95%. The grain size for this polycrystalline cobalt sample was determined by optical microscopy of the etched surface to be of the order of 100 μm. The other two working electrodes used were obtained from electrodeposited nanocrystalline Co and Co-P with grain sizes of 67 and 50 nm, respectively, as determined by the X-ray line broadening method.

The electrode surfaces were polished with progressively finer grades of abrasive, starting with emery paper and finishing with alumina powder with a grit size of 0.05 pm within 1 h of the electrochemical testing. The

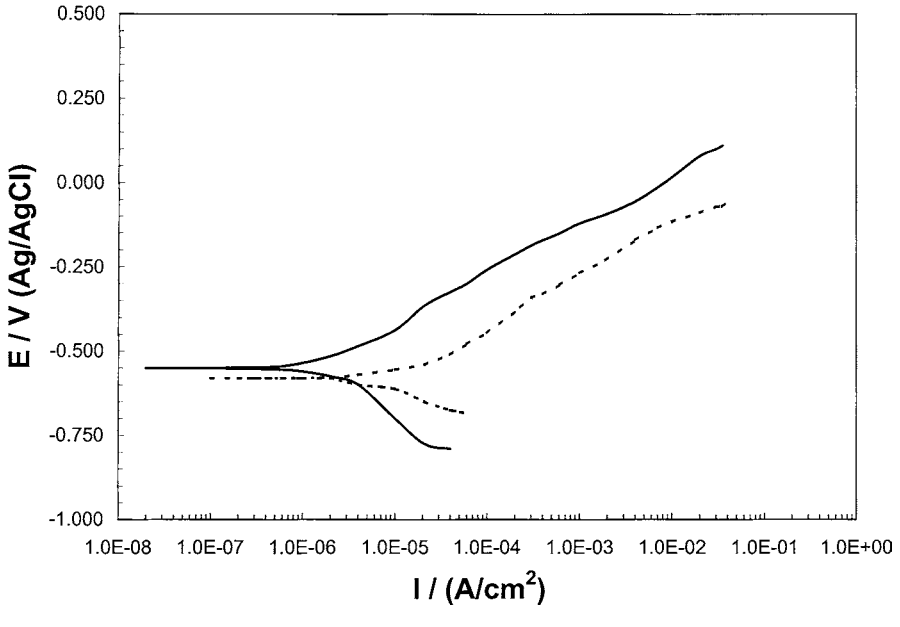

Figure 1 Potentiodynamic anodic polarization curves for the nanocrystalline Co (67 nm) (----) and conventional polycrystalline Co (100 μm) (___).

* Author to whom all correspondence should be addressed.

0022–2461 © *2004 Kluwer Academic Publishers*

surfaces were rinsed and thoroughly degreased with ethanol before introduction into the electrolyte solution [ASTM standard G5-82].

The electrolyte used to study the anodic potentiodynamic polarization behavior was 0.25 M Na_2SO_4 at room temperature and pH 10.5. 300 ml of electrolyte were used for each test and the oxygen level of the solution was reduced with bubbling N_2 gas 15 min before and during the test. Potentiodynamic anodic polarization tests were then conducted by stepping the potential at a scan rate of 0.5 mV/s from −800 mV to 200 mV (vs. Ag/AgCl reference electrode).

Corrosion testing was conducted using Autolab potentiostat/galvanostat (PGSTAT 100) with a compliance voltage of 100 V and maximum current 250 mA. A standard corrosion cell containing the working electrode, two platinum counter electrodes and a Ag/AgCl/Cl^- (3M KCl) reference electrode. The General Purpose Electrochemical System (GPES) software model 4.8 with a personal computer in conjunction with the Autolab was used as a data acquisition system. The surface morphology of the corroded samples was studied by scanning electron microscopy (SEM) using a Jeol 6400 scanning electron microscope.

The potentiodynamic testing has been undertaken in order to evaluate the bulk corrosion behavior of electroplated nanocrystalline Co and Co-P (coating thickness is 15–20 μm) in alkaline media in comparison to electrowon conventional polycrystalline Co.

The potentiodynamic polarization curves for the nanocrystalline Co (67 nm) specimen as well as large grained (100 μm) conventional polycrystalline Co are shown in Fig. 1. Some of the key electrochemical parameters extracted from Fig. 1 appear in Table I.

It is clear from Fig. 1 that the nanocrystalline and conventional polycrystalline Co exhibit active behavior and did not passivate. In the curve for polycrystalline Co, the free corrosion potential, E_{corr}, was observed at −0.547 V (Ag/AgCl). As the potential was increased, the polycrystalline Co specimen entered the active corrosion regime, as seen by the increasing current with potential. The nanocrystalline Co showed the same active behavior as that observed for polycrystalline Co. The free corrosion potential, E_{corr}, for nanocrystalline Co was observed at −0.574 V (Ag/AgCl). The nanocrystalline Co specimen shows more cathodic potential than that of the conventional polycrystalline Co. This is in contrast to the nanocrystalline pure Ni system studied by Rofagha *et al*. [8]. The authors reported that there is a significant anodic shift in E_{corr} for the nanocrystalline Ni with respect to its conventional crystalline counterpart. This was interpreted to be the result of the enhanced catalysis of the hydrogen reduction reaction at the surface of nanocrystalline Ni due to the large quantity of intercrystalline defects such as grain boundaries and triple junctions. This inconsistency is probably due to the difference in crystalline

TABLE I Key electrochemical parameters for polycrystalline Co, nanocrystalline Co and nanocrystalline Co-P specimens extracted from Figs 1 and 3

Material	Grain size	E_{corr} V (Ag/AgCl)	i_{corr} A/cm^2
Nanocrystalline Co	67 nm	−0.574	0.860×10^{-6}
Polycrystalline Co	100 μm	−0.547	1.847×10^{-6}
Nanocrystalline Co-P	50 nm	−0.581	19.330×10^{-6}

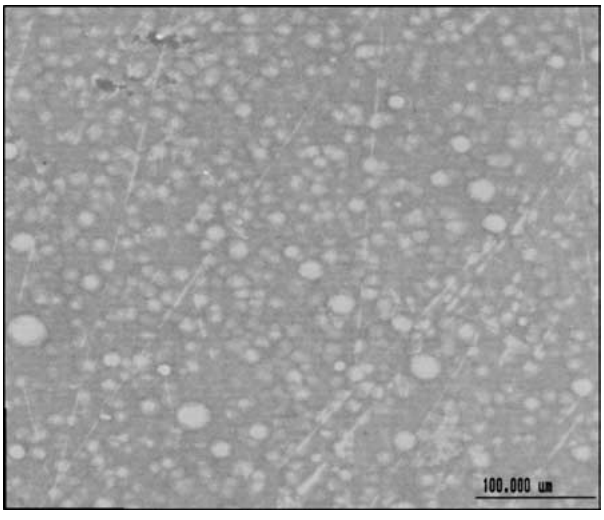

(a)

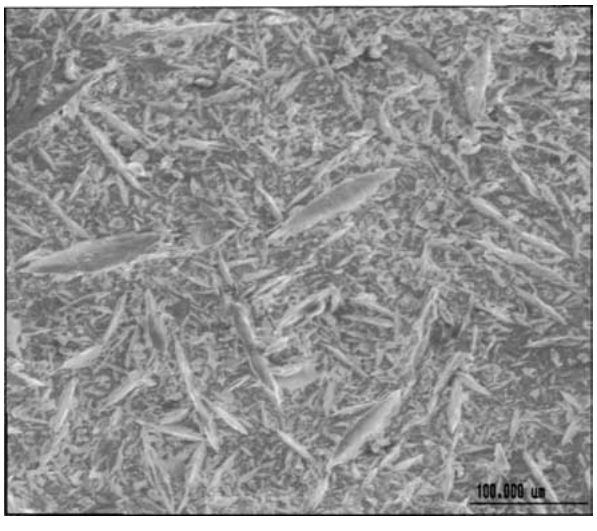

(b)

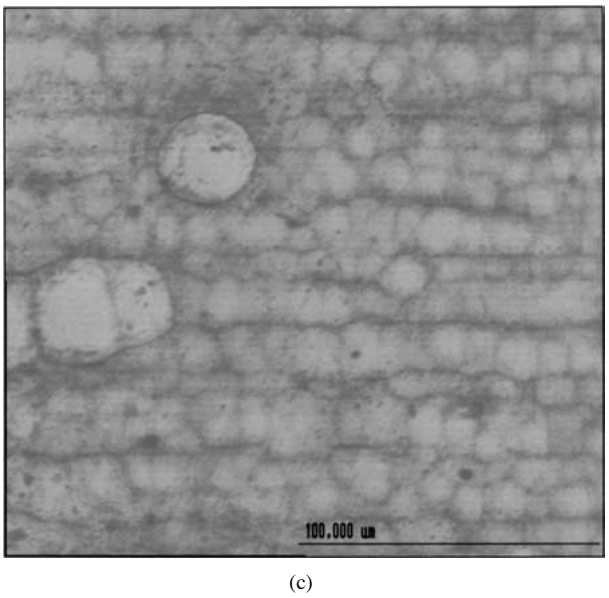

(c)

Figure 2 Scanning electron micrographs of (a) nanocrystalline Co (67 nm), (b) polycrystalline Co (100 μm) and (c) nanocrystalline Co-P (50 nm), following anodic polarization tests.

structure between Ni and Co. Like many other transition metals, the cobalt surface is covered by a native barrier film, which consists mainly of CoO or hydrated oxide $CoOH_2O$ [16]. Indeed, the potentiodynamic polarization of the polycrystalline cobalt and cobalt-based alloys has been reported on numerous occasions. For example, Badawy *et al*. [17] studied the anodic polarization of the conventional cobalt in acidic, neutral and alkaline solutions. They considered that in acidic solutions, the passive film is unstable and hence higher rates of corrosion were recorded. This corrosion process is preceded by a pure chemical dissolution of the native cobalt oxide, CoO, or the hydrated oxide, $CoOH_2O$. They described the dissolution process by:

$$CoO + 2H^+ \rightarrow Co^{2+} + H_2O \quad (1)$$

$$Co(OH)_2 + 2H^+ \rightarrow Co^{2+} + 2H_2O \quad (2)$$

In neutral and alkaline solutions stabilization of the passive film occurs whereas in acidic solution reactivation of the passive film is taking place as described by Equations 1 and 2.

Since there are no significant differences between the chemical compositions of the nanocrystalline and polycrystalline Co, it can be speculated that the cathodic shift of nanocrystalline Co may be due to the microstructural differences (i.e. intercrystalline volume fraction) between the nanocrystalline and conventional polycrystalline Co. In the low potential region, corrosion attack is initiated more easily at defects sites (i.e. grain boundaries and triple junctions). The higher volume fraction of the intercrystalline constituent in nanocrystalline materials provides active sites due to the fact that grain boundaries and triple junctions possess higher energies than the crystal surface.

Scanning electron micrographs of the nanocrystalline and polycrystalline Co taken after potentiodynamic anodic polarization scans are presented in Fig. 2. The nanocrystalline specimen (Fig. 2a) showed excessive uniform corrosion, while less of the same type of corrosion was observed for the polycrystalline specimen (Fig. 2b). The surface of both specimens was found to be covered by a porous, non-protective film.

Fig. 3 shows the anodic polarization curves for nanocrystalline Co-P (50 nm) specimen as well as conventional polycrystalline Co. The open circuit potentials (E_{corr}) and the corrosion current density (i_{corr}) extracted from Fig. 3 as well as the grain size of the Co and Co-P appear in Table I. Nanocrystalline Co-P shows active behavior and did not passivate and had a free corrosion potential, E_{corr}, at -0.581 V (Ag/AgCl).

The free corrosion potential (E_{corr}) of the nanocrystalline Co-P specimen is found to be more cathodic than that of the conventional Co. This is similar to nanocrystalline pure Co system discussed previously in which there was higher volume fraction of the intercrystalline constituent in nanocrystalline materials provides active sites. This observation that nanocrystalline Co-P is more cathodic than that of the conventional Co is consistent with Ni-P (8.4 nm) specimen with respect to conventional Ni [12]. Rofagha *et al*. assessed the corrosion behavior of nanocrystalline electroplated Ni-P alloys having grain sizes of about 8 nm and 22 nm in 0.1 M H_2SO_4 using the potentiodynamic anodic polarization technique. The behavior of these nanocrystalline materials were also compared to amorphous Ni-P and coarse-grained (100 μm) polycrystalline pure Ni. The open circuit potential (E_{corr}) of the amorphous alloy was found to be more anodic than that of the conventional Ni, while one of the nanocrystalline Ni-P specimens (8.4 nm) displayed a more cathodic open circuit potential. However, they suggested that no clear correlation between E_{corr} and microstructure was evident. They attributed this behavior mainly to the hydrogen evolution exchange current being influenced by the presence of P.

The scanning electron micrograph presented in Fig. 2c shows the morphology of the nanocrystalline Co-P specimen following the potentiodynamic anodic

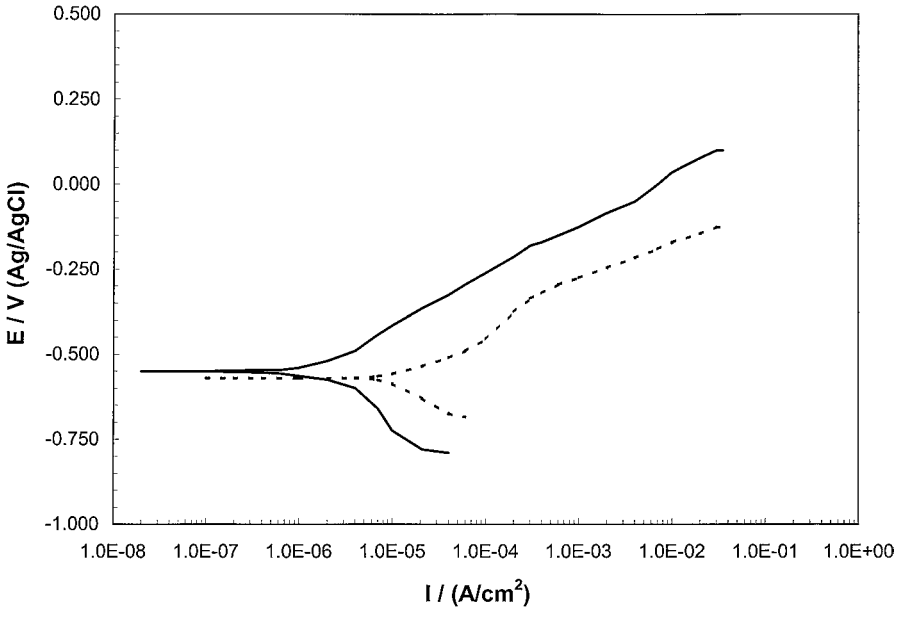

Figure 3 Potentiodynamic anodic polarization curves for the nanocrystalline Co-P (50 nm) (----) Specimen and conventional polycrystalline Co, 100 μm, (___).

polarization scans. The nanocrystalline Co-P specimen shows the same behavior as the pure nanocrystalline Co, i.e. excessive uniform corrosion, while the polycrystalline Co specimen (Fig. 2b) showed less uniform corrosion.

In conclusion, the nanocrystalline Co and Co-P exhibit active behavior and did not passivate. Nanocrystalline Co and Co-P specimens show more cathodic potential than that of their conventional polycrystalline Co and The free corrosion potential, E_{corr} of nanocrystalline Co and Co-P were observed at -0.574 and -0.581 V (Ag/AgCl) respectively. Scanning electron micrographs of the nanocrystalline and polycrystalline Co showed excessive uniform corrosion in nanocrystalline specimen, while less of the same type of corrosion was observed for the polycrystalline Co. The nanocrystalline processing of Co provides considerable promise for the development of coatings for corrosion protection.

Acknowledgment

Financial support by the Natural Sciences and Engineering Research Council of Canada (NSERC) and Integran Technologies Inc. is gratefully acknowledged.

References

1. UK Chromium Plating Regulations 1931 (amended in 1973), HMSO (1073).
2. HSE Toxicity Review, TR31, HMSO (1989).
3. Metals Handbook.
4. MIL-P-6871 (2), 1955.
5. J. K. DENNIS and T. E. SUCH, "Nickel and Chromium Plating" 3rd edn. (Woodhead Publishing Ltd., Cambridge, UK, 1993).
6. A. M. EL-SHERIK, U. ERB, G. PALUMBO and K. T. AUST, *Scripta Metall. Mater.* **27** (1992) 1185.
7. M. J. AUS, B. SZPUNAR, A. M. EL-SHERIK, U. ERB, G. PALUMBO and K. T. AUST, *ibid.* **25** (1992) 3027.
8. R. ROFAGHA, R. LANGER, A. M. EL-SHERIK, U. ERB, G. PALUMBO and K. T. AUST, *ibid.* **25** (1991) 2867.
9. *Idem.*, *Mat. Res. Soc. Symp. Proc.* **238** (1992) 751.
10. G. PALUMBO, U. ERB and K. T. AUST, *Scripta Metall. Mater.* **24** (1990) 2347.
11. R. ROFAGHA, S. J. SPLINTER, U. ERB and N. S. MCINTYRE, *NanoStruct. Mater.* **4**(1) (1994) 69.
12. R. ROFAGHA, U. ERB, D. OSTRANDER, G. PALUMBO and K. T. AUST, *ibid.* **2** (1993) 1.
13. S. J. SPLINTER, R. ROFAGHA, N. S. MCINTYRE and U. ERB, *Surf. Interf. Anal.* **24** (1996) 181.
14. S. WANG, R. ROFAGHA, P. R. ROBERGE and U. ERB, *Electrochem. Soc. Proc.* **95**(8) (1995) 244.
15. U. ERB and A. M. EL-SHERIK, U.S. Patent 5,352,266 (1994).
16. M. POURBAIX, "Atlas of Electrochemical Equilibrium Diagrams in Aqueous Solutions" (NACE, Houston, Texas, 1966) p. 322.
17. W. A. BADAWY, F. M. AL-KHARAFI and J. R. AL-AJMI, *Bulletin of Electrochemistry*, **16** (2000) 145.

Received 24 February
and accepted 31 July 2003